# Heat and Mass Transfer Effects on Passive Control MHD Flow of Nanoparticles with Variable Thermophysical Properties

BEAUTY B. MALEMI[1], KELVIN. O. OGBORU[2], AKINDELE M. OKEDOYE[3]
[1, 2, 3] *Department of Mathematics, Federal University of Petroleum Resources, Effurun, Nigeria*

***Abstract-*** ***Passive flow control techniques, and particularly vortex generators have been used successfully in a broad range of aero- and hydrodynamics applications to alter the characteristics of boundary layer separation. To analyse Heat and Mass Transfer Effects on Passive Control MHD Flow of Nanoparticles with Variable Thermophysical Properties, Buongiorno's model incorporated with variable thermal conductivity and viscosity. The resulting nonlinear coupled partial differential equation was transformed to dimensionless system to determine the flow governing parameters and solved using an efficient built-in routine of maple 2021. The result shows that increase in heating of the plate results in decrease in velocity while velocity increases during cooling of the plate. We also discovered that increase in injection reduces the velocity while increase in the suction increases the velocity. Generative chemical reaction parameter enhances chemical species concentration. An increase in Brownian motion parameter brings about decline in specie concentration. Comprehensive analysis of the study were presented with graphs and discussed. It could be concluded that passive control of flow could be used to maximize the efficiency of engineering design.***

***Indexed Terms-*** ***Buoyancy Medium, Nanoparticles, MHD Flow, Passive Control, Porous, Thermophysical properties***
***2020 MCS Classification—76A05, 76D05, 76W05***

## I. INTRODUCTION

Flow control is a major rapidly evolving field of fluid dynamics. It implies a small change of a configuration serving large engineering benefit, like drag reduction, lift increase, mixing enhancement or noise reduction. This change may be accomplished by passive devices like turbulators or roughness elements which are steady and require no energy by definition. Airplane wing performance has a substantial effect on not only the runway length, approach speed, climb rate, cargo capacity, and operation range but also the community noise and emission levels. The wing performance is often degraded by flow separation, which strongly depends on the aerodynamic design of the airfoil profile.

Passive flow control method require no auxiliary power and no control loop [1]. Passive techniques include geometric shaping, the use of vortex generators, and the placement of longitudinal grooves or riblets on airfoil surfaces. A passive dissipation device utilizes the motion of the structure to generate the control force (no external power source needed). In the following, it will be mainly focused on fluid viscous dampers i.e. FVD, and their design optimization, which is seen as intensive task, all illustrated with an example.

Friction damper consists of four links located at the intersection of cross bracings (tension brace and compression brace) [2]. A slippage is permitted for one of the braces then the other slips, which allow the device to dissipate energy in both braces. Filiatrault and Cherry [3] tested and confirmed that this type of devices can increase substantially the capacity of dissipation in one cycle and reduce the amount of drifts. However [4], cited some reliability issues that concerns this sliding option, which can change the interface condition with time, and since their behavior is highly nonlinear, it may provoke undesirable structural behavior by exciting higher modes.

Metallic damper or also called yielding steel elements, many concepts are proposed, it can consist on round steel bar integrated in the bracing frame ([5], [6] and

[7]), with their stable hysteretic behavior and reliability for long periods, they also present an insensitivity to temperature. One must mention that after a severe excitation, this device may be severely damaged and must be replaced.

It was reported that external airborne installations of cylindrically-shaped objects, such as turrets, can lead to severe degradation of flight performance. This engineering challenge is mainly due to an unsteady and separated vortex flow field that evolves in the wake downstream of the turret [8]. Their reveal an engineering solution to attenuate the wake unsteadiness. An experiment in the Israeli Air Force (IAF) low speed wind tunnel was conducted [8], where they investigated various passive flow control methods on a hemispherical dome attached to a cylindrical body turret with a low aspect ratio (AR) of 1.36 at a diameter-based Reynolds number of $Re_D = 3.75 \times 10^5$. The results show that tripping the flow using a bump strip is the most effective for the turret studied herein.

For the purpose of improving the performance of trajectory tracking for quadrotors with the control input saturation, a novel model-free saturated prescribed performance reinforcement learning framework is proposed in the presence of the model uncertainties, nonlinearities and external disturbances [9]. Saturation functions are employed to deal with input saturation, and the actuator's saturation nonlinearity is compensated by an intelligent method to decrease the saturation effects. And the prescribed performance control is utilized to ensure an adjustable transient and steady state response for the tracking errors.

Waverider is expected to break the lift-to-drag ratio constraint in the hypersonic flight condition and it is commonly been studied as the forebody of the cruise vehicle. An approach to make Waverider as the airframe for the air-breathing cruise vehicle was developed [10]. The fuselage that designed based on the cone-derived Waverider theory with a unique upper boundary curve generates the same conical shock wave as that generated by the conical nose of the vehicle. Therefore, the vehicle is expected to have a full-body wave-ride performance and suitable for cruising in the hypersonic condition. Their results show that the increase of the design Mach number does negative impact on the lift-to-drag ratio but positive impact on the volumetric efficiency while the increase of the design direction angle has an opposite influence. Zonghan et al. [11] presents a novel design method of pressure-controllable bump for hypersonic aircraft fore-body. The method can effectively resolve the tradeoff among boundary layer diversion, flow uniformity, and external drag reduction. The classical permeable-boundary method is improved by coupling with the radius-based function, through which the prescribed surface pressure distribution can inversely generate the bump. Compared with the typical streamline-tracing bump, the new bump is 44.9% lower in height while diverting identical low kinetic energy flow. According to the space occupied with high kinetic energy flow, the uniform region to preset the inlet of the new bump is 58.0% wider than that of the typical bump. Their research confirms that the new pressure-controllable bump shows better integrating capacity with the hypersonic inlets than the typical bump.

Control of the boundary layer upstream and in the region of the engine inlet is an important consideration for airplane designers. With a large offset between the flush entrance and the compressor face, these low drag concepts are suitable for stealth applications, but when the wetted area upstream of the inlet is long, the ingestion of thickened boundary layer results in flow separation at the bends, pressure recovery losses and finally reduction of thrust[12].

Experimental testing and validated CFD models have been used to evaluate the performance of the FC4GT flameless gas turbine (GT) combustor operating at a global equivalence ratio of 0.44. The methane-fuelled combustor was tested at atmospheric pressure, modelled at elevated pressures up to 25 bar, and optimised for a combustor pressure of 15 bar. The combustor was analysed for firing rates between 15 kW and 16 MW, which correspond to heat density range between 0.15 MW/m3.bar and 150 MW/m3.bar, respectively[13].

Tiancai et al. [14] proposes a performance-focused and deep learning-based hierarchical fault-tolerant control framework for over-actuated hypersonic reentry vehicles. The hierarchical fault tolerance

mechanism refers to the fault tolerance that can be realized both in the control allocation and control layers.

In many practical situations nowadays, there are situations in which we have to work out with different types of nanoparticles. These nano sized particles play a crucial role in controlling the different thermo physical properties of different fluids involved. Most of the fluids in practice such as water, ethylene, glycol, kerosene oil, engine oil are the poor conductors of heat. Lower values of thermal conductivity and other thermal properties is a major factor for this. To cope with this problem and to enhance the thermal properties of these fluids, nanoparticles are added to the base fluids. Many researchers studied and proposed various models to get a concrete analysis of these nanoparticles based nanofluids. The classical Stokes' problem is the investigation of diffusion of vorticity over a suddenly moved flat surface [15]. Rajagopal and Na [16] extended the traditional problem for the case of non-Newtonian fluid. Over the years, many researchers studied several properties of velocity field in Stokes' problem. Many studies can be seen in literature on Stokes' problem [17]–[32]. Recently, after the pioneering works in nanofluids, Naseem Uddin et al. [33] presented a study of nanofluids due to a suddenly moved plate. Rosali et al. [34] used the Buongiorno model to study the effects of Brownian motion and thermophoresis on heat and mass transfer in nanofluids.

In a recent study, Nield and Kuznetsov [35]–[37] presented a new revised model that in cooperated the zero flux boundary condition for concentration profile at the wall. This boundary condition includes the effects of Brownian motion and thermophoresis so that the nanofluid particle fraction can be passively controlled at the wall. They also commented that this model is more realistic physically as compared to earlier models. In work of Syed et al.[38], the model presented by Nield and Kuznetsov [35]–[37] is used to investigate the flow behavior of a nanofluid over a suddenly moved flat plate. Effects of Brownian motion and thermophoresis are incorporated in the zero flux boundary condition. The effect of buoyancy, Lorentz force, heat source, chemical reaction were neglected. Hence, in this work, we wish to carry out investigation into Heat and Mass Transfer Effects on MagnetoHydroDynamic Flow of Nanoparticles with Buoyancy and Variable Viscousity and Thermal Conductivity by extending the work of Syed et al. [38] to include buoyancy, Lorentz force, heat source, chemical reaction as well as Variable Viscousity and Thermal Conductivity. This study is different from some of the previous studies as the effects of Brownian motion and thermophoresis on nanoparticles volume fraction are passively controlled on the boundary rather than actively.

## II. GOVERNING EQUATIONS

Consider the flow of a Newtonian nanofluid lying over an impulsively started heated plate. Cartesian coordinate system is taken to describe the flow behavior. $x$ and $y$ respectively are the coordinates along and normal to the plate. Initially (at time $t = 0$), the plate is starts moving with a constant velocity $U_\infty$. The plate is kept at a constant temperature $T_w$, and the nanoparticle volume fraction $C_w$. At a large distance from the plate, the temperature and the nanoparticle volume fraction are represented by $T_\infty$ and $C_\infty$, respectively. A uniform time dependent transverse magnetic field is applied in y-direction. Strength of magnetic field is taken to be $B = B_0$. Induced magnetic field is assumed to be very small as compared to the applied magnetic field and is neglected. Figure 1 shows the schematic diagram for the flow problem.

The following model assumptions, the governing equations of the model are derived:

(1) All fluid properties except density in the thermal and concentration buoyancy force term are constant.
(2) The influence of the density variations in other terms of the momentum, energy and concentration
equations are negligible.
(3) The Eckert number Ec and the magnetic Reynolds number are small so that the induced magnetic field can be neglected.
(4) The external electric field is supposed to be zero.
(5) All the physical variables are functions of $y$ and $t$ only.

Therefore, the only velocity component is in $y$ -direction. By above assumption, the continuity equation could be written as

$$\frac{\partial v}{\partial y} = 0 \tag{1}$$

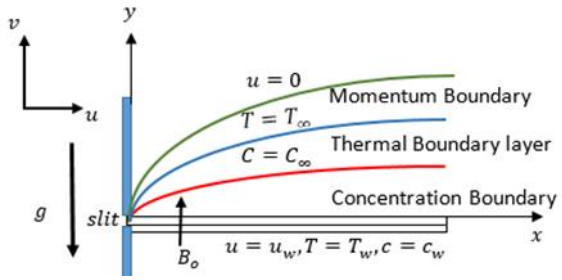


Figure 1 Schematic diagram for the flow problem

Under the Boussinesq's approximation, the fluid momentum, energy and species equations in the neighbourhood of the plate is described by the following respectively

$$\rho_f\left(\frac{\partial u}{\partial t} + v\frac{\partial u}{\partial y}\right) = -\frac{\partial p}{\partial x} + \frac{\partial u}{\partial y}\left(\mu_T\frac{\partial u}{\partial y}\right) + g\beta_T(T - T_\infty) + g\beta_C(C - C_\infty) - \sigma B_0^2 u \tag{2}$$

$$\rho C_p\left(\frac{\partial T}{\partial t} + v\frac{\partial T}{\partial y}\right) = \frac{\partial T}{\partial y}\left(K_T\frac{\partial T}{\partial y}\right) + \tau\left[D_B\left(\frac{\partial C}{\partial y}\frac{\partial T}{\partial y}\right) + \left(\frac{D_T}{T_\infty}\right)\left(\frac{\partial T}{\partial y}\right)^2\right] + Q(T - T_\infty) \tag{3}$$

$$\frac{\partial C}{\partial t} + v\frac{\partial C}{\partial y} = D_B\left(\frac{\partial^2 C}{\partial y^2}\right) + \frac{D_T}{T_\infty}\left(\frac{\partial^2 T}{\partial y^2}\right) + A(C - C_\infty). \tag{4}$$

where, $u$ is the velocity component along the $y$ −axis, $U_\infty$ is the free stream velocity, $\rho_f$ is the density of base fluid, $v = \mu_f/\rho_f$ is kinematic viscosity, $\sigma$ is electrical conductivity, $B_0$ magnetic field flux density, $\alpha$ thermal diffusivity, $D_B$ is Brownian motion diffusion coefficient, $D_T$ thermophoresis diffusion coefficient, $T$ and $C$ are fluid temperature and nanoparticle volume fraction, respectively, $\tau$ is the parameter defined by $\frac{(\rho c)_f}{(\rho c)_p}$,

where $(\rho c)_f$ is the heat capacity of the nanofluid and $(\rho c)_p$ is the effective heat capacity of the nanoparticle material.

MHD Boundary Layer Flow Past a Moving Plate with Mass Transfer and Binary Chemical Reaction was investigated by [39] and [40], while the variation in viscosity and thermal conductivity due to internal friction between the surface and fluid particle have to be taken into account, it is appropriate to assumed the mathematical formulation of the thermal conductivity and viscosity dependents on temperature as investigated in [41 and [42**]**. We assume the viscousity and thermal conductivity similar to the used by Wahab et al.[43]:

$$\begin{aligned} \mu_T &= \mu_f\big(a + b_1(T_\infty - T)\big) \\ k_T &= k_f\big(a_1 + b_2(T - T_\infty)\big)' \end{aligned} \tag{5}$$

The initial and boundary conditions for passive control model are:

$$\begin{aligned} t < 0:&\quad u = 0, v = v_w, T = T_w, C = C_w, \forall\, y \\ t \geq 0:&\begin{cases} u = U_0, v = v_w, T = T_w \\ D_B\frac{\partial C}{\partial y} + \frac{D_T}{T_\infty}\frac{\partial T}{\partial y} = 0 \end{cases}, \text{at } y = 0 \\ &\begin{cases} u \to 0, T \to T_\infty, C \to C_\infty, & \text{as } y \to \infty \end{cases} \end{aligned} \tag{6}$$

it is pertinent to mention that the last part of the boundary condition (6) takes the thermosphoresis into account and normal flux of the nanofluid at the boundary is taken to be zero [21]–[23]. The major purpose of this condition is the passive control of nanoparticle volume fraction at the boundary. This condition is different from the earlier studies and gives a more realistic approach.

2.1 non-Dimensionlisation

For mathematical analysis of the problem for active control model, we use following non-dimensional variables

$$\left.\begin{aligned} &y' = \frac{y}{\delta}, u' = \frac{u}{U_0}, v' = \frac{v}{U}\frac{L}{\delta},\ t' = t\frac{U_0}{L}, \\ &p' = \frac{p}{\rho U^2}, U' = \frac{U}{U_0}, \omega' = \frac{4\omega L}{U_0}, V = \frac{U_1}{U_0}, \\ &\frac{(T - T_\infty)E_a}{R_G T_\infty^2} = \theta(t, y), \frac{(C - C_\infty)}{(C_w - C_\infty)} = \phi(t, y) \end{aligned}\right\} \tag{8}$$

At free stream

$$u \to U(t) = 1 + nt, T \to T_\infty, C \to C_\infty$$

Where is a parameter defined by

$$n = \frac{4\rho_f U_0 G}{L\sigma B_0^2 + 4\rho_f U_0}$$

$$\rho_f\left(\frac{\partial U}{\partial t}\right) = -\frac{\partial p}{\partial x} - \sigma B_0^2 U, \quad (9)$$

Equation (9) implies

$$-\frac{\partial p}{\partial x} = \rho_f\left(\frac{\partial U}{\partial t}\right) + \sigma B_0^2 U \quad (10)$$

Hence by equation (10), equation (2) becomes

$$\frac{\partial\theta(t,y)}{\partial t'} + v'\frac{\partial\theta(t,y)}{\partial y'} = \frac{1}{Pr}\frac{\partial}{\partial y'}\left(\left(\alpha + \varphi\theta(t,y)\right)\frac{\partial\theta(t,y)}{\partial y'}\right) + \frac{\pi}{\sigma(t)^2}\left[Nb\left(\frac{\partial\phi(t,y)}{\partial y'}\frac{\partial\theta(t,y)}{\partial y'}\right) + Nt\left(\frac{\partial\theta(t,y)}{\partial y'}\right)^2\right] + \frac{\beta}{Pr}\theta(t,y) \quad (12)$$

$$\frac{\partial\phi(y)}{\partial t'} + v'\frac{\partial\phi(y)}{\partial y'} = \frac{1}{Sc\sigma(t)^2}\frac{\partial^2\phi(y)}{\partial y'^2} + \frac{1}{Sc\sigma(t)^2}\frac{Nt}{Nb}\frac{\partial^2\theta(y)}{\partial y'^2} + \Lambda\phi(y) \quad (13)$$

$$\frac{\partial u'}{\partial t'} + v'\frac{\partial u'}{\partial y'} = \frac{dU'}{dt} + \frac{\nu}{\sigma(t)^2}\frac{\partial}{\partial y'}\left(\left(\zeta - \gamma\theta(t,y)\right)\frac{\partial u'}{\partial y'}\right) + Grt(\theta(t,y) + N\phi(t,y)) - M(u' - U') \quad (14)$$

The initial and boundary conditions for passive control model becomes:

$$u'(t,0) = 1, v'(t,0) = s, \theta(t,0) = 1, \quad Nb\frac{\partial\phi(t,0)}{\partial y'} + Nt\frac{\partial\theta(t,0)}{\partial y'} = 0 \quad (15)$$
$$u' \to 0, \theta(t,y) \to 0, \phi(t,y) \to 0, \text{as } y' \to \infty$$

Dropping primes, system of equations (12) – (14) together with the boundary condition (15) in non-dimensional form of the governing equations in terms of dimensionless variables are:

$$\frac{\partial v}{\partial y} = 0 \quad (16)$$

$$\left.\begin{aligned}\frac{\partial u}{\partial t} + v\frac{\partial u}{\partial y} &= \frac{dU}{dt} - M(u - U) + Grt(\theta(t,y)) \\ &+ \frac{\nu}{\sigma(t)^2}\frac{\partial}{\partial y}\left(\left(\zeta - \gamma\theta(t,y)\right)\frac{\partial u}{\partial y}\right) + N\phi(t,y))\end{aligned}\right\} \quad (17)$$

$$\rho_f\left(\frac{\partial u}{\partial t} + v\frac{\partial u}{\partial y}\right) = \rho_f\left(\frac{\partial U}{\partial t}\right) + \frac{\partial u}{\partial y}\left(\mu_T\frac{\partial u}{\partial y}\right) + g\beta_T(T - T_\infty) + g\beta_C(C - C_\infty) - \sigma B_0^2(u - U), \quad (11)$$

Using equation (8) in equations (1), (3), (4) and (11) respectively, we have

$$\frac{\partial v'}{\partial y'} = 0 \quad (11)$$

$$\frac{\partial\theta(t,y)}{\partial t} + v\frac{\partial\theta(t,y)}{\partial y} = +\frac{\beta}{Pr}\theta(t,y) + \frac{1}{Pr}\frac{1}{\sigma(t)^2}\frac{\partial}{\partial y}\left(\left(\alpha + \varphi\theta(t,y)\right)\frac{\partial\theta(t,y)}{\partial y}\right) + \frac{\pi}{\sigma(t)^2}\left[Nb\left(\frac{\partial\phi(t,y)}{\partial y}\frac{\partial\theta(t,y)}{\partial y}\right) + Nt\left(\frac{\partial\theta(t,y)}{\partial y}\right)^2\right] \quad (18)$$

$$\frac{\partial\phi(y)}{\partial t} + v\frac{\partial\phi(y)}{\partial y} = \frac{1}{Sc\sigma(t)^2}\frac{\partial^2\phi(y)}{\partial y^2} + \frac{1}{Sc\sigma(t)^2}\frac{Nt}{Nb}\frac{\partial^2\theta(y)}{\partial y^2} + \Lambda\phi(y) \quad (19)$$

And the corresponding boundary conditions (15) becomes

$$u(t,0) = 1, v(t,0) = s, \theta(t,0) = 1, \quad Nb\frac{\partial\phi(t,0)}{\partial y'} + Nt\frac{\partial\theta(t,0)}{\partial y'} = 0 \quad (20)$$
$$u \to 0, \theta(t,y) \to 0, \phi(t,y) \to 0, \text{as } y \to \infty$$

Where the dimensionless variable are

$$\left.\begin{aligned}&\left(a + b_1(T_w - T_\infty)\right)\frac{L}{U_0} = \zeta, \frac{L}{U_0\rho c_p} = \pi, \\ &a_1\frac{L}{U_0} = \alpha, \frac{L\sigma B_0^2}{\rho_f U_0} = M, \frac{D_B}{\rho}\frac{L}{U_0} = \frac{1}{Sc}, \\ &s = \frac{v_w L}{U\delta}, \frac{k_0}{\rho c_p} = \frac{1}{Pr}, \frac{QL}{k_0 U_0} = \beta, \\ &\frac{AL}{\rho U_0} = \Lambda, , b_1\frac{R_G T_\infty^2 L}{E_a U_0} = \gamma, b_2\frac{R_G T_\infty^2}{E_a U_0} = \varphi, \\ &\frac{\tau D_B(C_w - C_\infty)}{\upsilon} = Nb, \frac{\tau D_T R_G T_\infty}{E_a \upsilon} = Nt \\ &g\beta_T\frac{R_G T_\infty^2 L}{E_a\rho_f U_0^2} = Grt, \frac{\beta_C(C_w - C_\infty)}{\epsilon T_\infty\beta_T} = N,\end{aligned}\right\} \quad (21)$$

$Nt$ and $Nb$ Brownian motion parameter and thermophoresis parameter, respectively.

2.2 Rate of Heat and Mass Transfer at the wall

The quantities of engineering interest are the local Nusselt number Nu and Sherwood number Sh. These parameters characterize the wall heat and nano mass transfer rates,

The quantities Skin friction, Nusselt and Sherwood Number are denoted by $c_f, Nu$ and $Sh$ respectively and are define as follows:

$$c_f = \frac{\tau_w}{\rho U_0^2}, \tag{22}$$

$$Nu = \frac{x q_w}{k_0(T_w - T_\infty)}, \tag{23}$$

$$Sh = \frac{x q_m}{D_B(C_w - C_\infty)} \tag{24}$$

where $\tau_w$ represents the skin friction along the surface, $q_w$ the heat flux and $q_m$ the concentration flux from the surface and are respectively given as

$$\begin{aligned} \tau_w &= \mu(T)\left[\left(1+\frac{1}{\beta c}\right)\frac{\partial u}{\partial y} + \frac{1}{\beta c^6}\left(\frac{\partial u}{\partial y}\right)^3\right]_{y=0}, \\ q_w &= \left[-k_T \frac{\partial u}{\partial y}\right]_{y=0}, \\ q_m &= \left[-D_B \frac{\partial C}{\partial y}\right]_{y=0} \end{aligned} \tag{25}$$

where $U_0$ $q_m$ and $q_w$, represents the wall shear stress, mass flux and heat transfer respectively.

Using Equation (5) and (25) in (22) – (24) we have

$$c_f = \frac{\mu(T)}{\rho_f U_0^2}\left[\left(1+\frac{1}{\beta c}\right)\frac{\partial u}{\partial y} + \frac{1}{\beta c^6}\left(\frac{\partial u}{\partial y}\right)^3\right]_{y=0}, \tag{26}$$

$$Nu = \frac{x E_a}{k_0 R_G T_\infty^2}\left[-k_T \frac{\partial T}{\partial y}\right]_{y=0}, \tag{27}$$

$$Sh = \frac{x}{D_B(C_w - C_\infty)}\left[-D_B \frac{\partial C}{\partial y}\right]_{y=0} \tag{28}$$

Using equation (8), equations (26)-(28) are transform in dimensionless form as follows

$$c_f = \frac{1}{\delta^2}\left(\zeta - \gamma\theta(t,y)\right)\left[H\frac{\partial u'}{\partial y'} + \Omega\left(\frac{\partial u'}{\partial y'}\right)^3\right]_{y=0} \tag{29}$$

Also

$$Nu = -\frac{1}{\delta^2}\left[\left(\alpha + \varphi\theta(t,y)\right)\frac{\partial\,\theta(t,y)}{\partial y'}\right]_{y=0} \tag{30}$$

$$Sh = -\frac{1}{\delta}\left[\frac{\partial\phi(y,t)}{\partial y'}\right]_{y=0} \tag{31}$$

Where

$$\left(1+\frac{1}{\beta c}\right)\frac{1}{L} = H, \frac{U_0^2}{\beta c^6 L} = \Omega \tag{32}$$

2.3 Similarity Transformations

Integrating equation (17) we have

$$v(y,t) = contant$$

At $y = 0$,

$$v(0,t) = s = contant$$

That is

$$v(y,t) = V_w \tag{33}$$

Define similarity transformations

$$\begin{aligned} \eta = \frac{y}{\sigma(t)}, u(t,y) = U_0 f(\eta), \\ \theta(t,y) = g(\eta), \phi(t,y) = h(\eta) \end{aligned} \tag{34}$$

Where

$$\delta(t) = \frac{\sigma_0}{\sigma(t)}$$

Equation (18)-(20) becomes

$$\left.\begin{aligned} -\left(\eta\frac{\sigma(t)}{\nu}\frac{d\sigma(t)}{dt} - s\sigma(t)\right)f'(\eta) = \\ \frac{\sigma(t)^2}{\nu U_0}\frac{dU}{dt} + \frac{\partial}{\partial\eta}\left(\left(\zeta - \gamma\theta(\eta)\right)f'(\eta)\right) \\ +Grt(\theta(\eta) + N\phi(\eta)) - M\left(f(\eta) - \frac{U}{U_0}\right) \end{aligned}\right\} \tag{35}$$

$$\left.\begin{aligned} -\left(\eta\frac{\sigma(t)}{\nu}\frac{d\sigma(t)}{dt} - s\sigma(t)\right)\theta'(\eta) = \\ \frac{1}{Pr}\frac{\partial}{\partial\eta}\left(\left(\alpha + \varphi\theta(\eta)\right)\theta'(\eta)\right) + \frac{\beta}{Pr}\theta(\eta) \\ \pi\left[Nb\left(\phi'(\eta)\theta'(\eta)\right) + Nt\left(\theta'(\eta)\right)^2\right] \end{aligned}\right\} \tag{36}$$

$$\left.\begin{aligned} -\left(\eta\frac{\sigma(t)}{\nu}\frac{d\sigma(t)}{dt} - s\sigma(t)\right)\phi'(\eta) = \\ \frac{1}{Sc}\phi''(\eta) + \frac{1}{Sc}\frac{Nt}{Nb}\theta''(\eta) + \Lambda\phi(\eta) \end{aligned}\right\} \tag{37}$$

The left hand-side of equations (35)-(37) suggest that

$$\frac{\sigma(t)}{\nu}\frac{d\sigma(t)}{dt} \text{ is a constant} \tag{38}$$

Integrating (38), we have

$$\sigma(t) = \sqrt{2c\nu t} \tag{39}$$

Wlog, we take $c = 2$ in (39). This implies

$$\sigma(t) = 2\sqrt{\nu t} \tag{40}$$

And

$$s = \frac{v_w L}{U\delta(t)} \Longrightarrow s\sigma(t) = \frac{v_w L}{U\delta(t)}\sigma(t) = \pm v_0 \quad (41)$$

Substituting the expression for $U(t)$ and equations (40) and (41) into equations (35)-(37), we then have well-posed non-linear governing equations for Heat and Mass Transfer Effects on MagnetoHydroDynamic Flow of Nanoparticles with Buoyancy and Variable Viscousity and Thermal Conductivity given as

$$\left.\begin{aligned}\frac{\partial}{\partial\eta}\Big(\big(\zeta - \gamma\theta(\eta)\big)f'(\eta)\Big) + (2\eta - v_0)f'(\eta)\\ +Grt\big(\theta(\eta) + N\phi(\eta)\big)\\ -M(f(\eta) - 1) + G = 0\end{aligned}\right\} \quad (42)$$

$$\left.\begin{aligned}\frac{\partial}{\partial\eta}\Big(\big(\alpha + \varphi\theta(\eta)\big)\theta'(\eta)\Big) + Pr(2\eta - v_0)\theta'(\eta)\\ \pi Pr\left[Nb\big(\phi'(\eta)\theta'(\eta)\big) + Nt\big(\theta'(\eta)\big)^2\right]\\ +\beta\theta(\eta) = 0\end{aligned}\right\} \quad (43)$$

$$\left.\begin{aligned}\phi''(\eta) + \frac{Nt}{Nb}\theta''(\eta) + Sc(2\eta - v_0)\phi'(\eta)\\ +\Lambda Sc\phi(\eta) = 0\end{aligned}\right\} \quad (44)$$

And the corresponding boundary conditions (16) becomes

$$f(0) = 1, \theta(0) = 1, Nb\frac{\partial\phi(0)}{\partial\eta} + Nt\frac{\partial\theta(0)}{\partial\eta} = 0 \quad (45)$$

$$f(\eta) \to 0, \theta(\eta) \to 0, \phi(\eta) \to 0, \quad \text{as } \eta \to \infty$$

Heat and Mass Transfer at the wall under the similarity transformation (34) becomes

$$c_f = \big(\zeta - \gamma\theta(\eta)\big)\left[Hf'(\eta) + \Omega\big(f'(\eta)\big)^3\right]_{\eta=0} \quad (45)$$

$$Nu = -\left[\big(\alpha + \varphi\theta(\eta)\big)\theta'(\eta)\right]_{\eta=0}, \quad (46)$$

$$Sh = -[\phi'(\eta)]_{\eta=0} \quad (47)$$

## III. METHOD OF SOLUTION

The system of coupled nonlinear equations. (42)–(44) subject to boundary conditions (45) is solved numerically by using an efficient built-in routine of MAPLE 2021. This command automatically converts the system of nonlinear equations into a set of initial value problems by employing the shooting technique and then solves the resulting system by using Runge-KuttaFehlberg method.

The dsolve command with the numeric option on a real-valued two-point boundary value problem (BVP), finds a numerical solution for the ODE or ODE system BVP. This type of BVP problem is automatically detected by dsolve, and an applicable algorithm is used. The optional equation method=bvp [traprich] was invoked to specify the BVP solver to be used. The method use Richardson extrapolation enhancement. For the enhancement schemes, Richardson extrapolation is generally faster, but deferred corrections uses less memory on difficult problems. This solution method is capable of handling BVPs with fixed, periodic, and even nonlinear boundary conditions as in our case. Our method provide an initial solution profile that approximately satisfies the boundary conditions.

We then use odeplot function to animates our solution curves obtained from the output (dsn) of a call to dsolve/numeric. The result of a call to odeplot is a PLOT data structure which is rendered by the plotting device.

## IV. RESULTS AND DISCUSSION

The flow of transient energy and concentration transport over a boundless moving vertical permeable flat sheet with chemical reaction, heat absorption or generation and suction has been formulated and solved analytically by asymptotic expansions. To get the influence of some entrenched terms on the reactive fluid flow, the subsequent description is considered. The default Prandtl number values is taken as $Pr = 0.71$ (plasma). The default Schmidt number value is picked as (0.60) to denote the water vapour. All emerging terms are mainly selected as follows: $\zeta = 1.2, \pi = 0.8, Grt = 5, M = 4, \Lambda = 0.5, \alpha = 0.5, v_0 = 0.2, Nb = 0.1, Nt = 0.1, N = 0.4, \beta = 0.6$ and $\varphi = 0.4$ except otherwise stated in each graph

The influence of each term on the mass, energy and flow rate distributions is displayed graphically. It should be noted that $Grt > 0$ and $Grt < 0$ depict the cooling and heating surface, respectively. Also, $\Lambda < 0$ and $\Lambda > 0$ represent generative and destructive chemical reactions, respectively. While $\beta < 0$ and $\beta > 0$ indicate heat generation and heat absorption, respectively.

### 4.1 Energy distribution

In Fig.2 it was observed that as injection parameter decreases the temperature decreases while, increase in suction parameter increases the temperature boundary

layer. It could also be seen from the graph that higher value of suction parameter enhances the temperature which should result in maximum temperature in the body of the fluid away from the wall. We observed that 100% increment in both injection and suction respectively produces 57.7% and 64.63% increment in temperature when the scaled distance is 1 unit from the wall. The effect of variable thermal conductivity and Brownian motion parameters was depicted in Fig.3 and Fig.4 respectively, it could be seen from the two figures that increase in both parameter enhances the temperature of the flow. We posited that200% and 400% increment in variable thermal conductivity and Brownian motion priduces34% and 25.6% respectively. Further 200% and 50% increment produces 42% and 22.6% respectively. But because of the passive control on the flow, this trend is not continuous as further 200% and 100% increment in both thermal conductivity and Brownian motion produced 34% and 35.29% increment respectively in temperature. From Fig.5 it was observed that as heat absorption increases temperature increases, whereas increase in heat generation reduces the temperature. A peak is observed at a higher value of heat absorption which indicate maximum that temperature occur in the body of the fluid. 62.56% increment in both heat generation and absorption yielded 44.5% and 35,8% increment respectively in temperature.

4.2 Concentration distribution

The effect of heat generation/absorption parameter on chemical specie concentration is shown in Fig.6, from the figure it could be seen that at about 0.25 unit from the wall increase in heat absorption enhances the chemical specie while between 0.25 unit to 1.25 unit from the wall increase in heat absorption reduces the chemical specie concentration and beyond 0.25 unit the reverse is the case. It could be seen that $0 \leq \eta < 0.5$ increase in heat generation decreases the chemical specie while $0.5 < \eta < \infty$ increase in heat generation increase the chemical specie concentration and beyond 0.25 unit the chemical specie concentration decreases. At about 0.4 unit from the wall in Fig.7, increase in thermal conductivity increases the chemical specie concentration beyond 0.4 unit increase in thermal conductivity parameter decreases the chemical specie concentration. The effect of chemical reaction parameter is depicted in Fig.8, as generative chemical reaction parameter decreases, chemical specie concentration decreases, the specie concentration boundary layer increases as destructive chemical reaction parameter increases. We display in Fig.9 the effect of Brownian motion parameter on the specie concentration, it could be seen that between 0.9 unit away from the wall as Brownian motion parameter increases, the specie concentration decreases. Beyond 1 unit away from the wall, as Brownian motion parameter increases, the specie concentration increases.

4.3 Velocity distribution

The effect of flow governing parameter on velocity distribution is shown in Fig.10 to Fig.17. Fig.10 shows the effect of thermal buoyancy on velocity, from the figure increase of heating of the plate result in decrease in velocity while velocity increases during cooling of the plate. Increase in the injection reduces the velocity while increase in the suction increases the velocity as shown in Fig.11. We display the effect of pressure gradient In Fig.12. It could be seen that as pressure gradient increases the velocity also increases. The effect of bulk thermal conductivity is displayed in Fig.13. It could be seen that as bulk thermal conductivity increases velocity also increases. As bulk viscosity and variable thermal conductivity increases as shown in Fig.14 and Fig.15, velocity also increases. In Fig 16, the effect of Hartmann number is displayed. It could be seen that as Hartmann number increase the velocity increases. As variable viscosity parameter increases as shown in Fig.17, the velocity increases.

- Wall Transfer Rate

The effect of transfer rate at the wall is shown in Table 1. From the values in the table, it could be seeing that decrease in $\beta$ reduces Sherwood and skin friction number while Nusselt number increases. As the Brownian motion parameter increases, Sherwood and skin friction number decreases, while Nusselt number increases. Increase in variable thermal conductivity increases the Sherwood and the skin friction number while the Nusselt number reduces. As the chemical reaction parameter increases, the Sherwood and the skin friction number reduces while the Nusselt number increases. Increase in the bulk thermal conductivity increases the Sherwood and the skin friction number while there is a decrease in the Nusselt number. As the suction/injection velocity increases the Sherwood and the skin friction numberincreases while the Nusselt

number decreases. While increase in the thermal buoyancy increases the skin friction. As Boyancy ratio increases, the skin friction reduces.

Table 1: Effect of governing parameters on the flow $\zeta = 1.2, \pi = 0.8, Grt = 5, M = 4, \Lambda = 0.5, \alpha = 0.5, v_0 = 0.2, Nb = 0.1, Nt = 0.1, N = 0.4, \beta = 0.6$

| $\beta$ | Grt | N | $\gamma$ | Nb | Nt | $\varphi$ | $\Lambda$ | $v_0$ | G | M | $Sh$ | $Nu$ | $c_f$ |
|---|---|---|---|---|---|---|---|---|---|---|---|---|---|
| 1.6 | 5.0 | 0.4 | 0.2 | 0.1 | 0.1 | 0.4 | 0.5 | 0.2 | -4.0 | 4.0 | 0.04084 | -0.36757 | -0.00449 |
| 0.6 | 5.0 | 0.4 | 0.2 | 0.1 | 0.1 | 0.4 | 0.5 | 0.2 | -4.0 | 4.0 | -0.04971 | 0.44739 | -0.09290 |
| -0.6 | 5.0 | 0.4 | 0.2 | 0.1 | 0.1 | 0.4 | 0.5 | 0.2 | -4.0 | 4.0 | -0.10709 | 0.96377 | -0.20105 |
| -1.6 | 5.0 | 0.4 | 0.2 | 0.1 | 0.1 | 0.4 | 0.5 | 0.2 | -4.0 | 4.0 | -0.14147 | 1.27321 | -0.28130 |
| 0.6 | -5.0 | 0.4 | 0.2 | 0.1 | 0.1 | 0.4 | 0.5 | 0.2 | -4.0 | 4.0 | -0.04971 | 0.44739 | -11.31270 |
| 0.6 | -2.0 | 0.4 | 0.2 | 0.1 | 0.1 | 0.4 | 0.5 | 0.2 | -4.0 | 4.0 | -0.04971 | 0.44739 | -4.79888 |
| 0.6 | 5.0 | 0.4 | 0.2 | 0.1 | 0.1 | 0.4 | 0.5 | 0.2 | -4.0 | 4.0 | -0.04971 | 0.44739 | -0.09290 |
| 0.6 | 10.0 | 0.4 | 0.2 | 0.1 | 0.1 | 0.4 | 0.5 | 0.2 | -4.0 | 4.0 | -0.04971 | 0.44739 | 0.33534 |
| 0.6 | 5.0 | 0.2 | 0.2 | 0.1 | 0.1 | 0.4 | 0.5 | 0.2 | -4.0 | 4.0 | -0.04971 | 0.44739 | -0.08982 |
| 0.6 | 5.0 | 0.8 | 0.2 | 0.1 | 0.1 | 0.4 | 0.5 | 0.2 | -4.0 | 4.0 | -0.04971 | 0.44739 | -0.09930 |
| 0.6 | 5.0 | 1.2 | 0.2 | 0.1 | 0.1 | 0.4 | 0.5 | 0.2 | -4.0 | 4.0 | -0.04971 | 0.44739 | -0.11127 |
| 0.6 | 5.0 | 1.6 | 0.2 | 0.1 | 0.1 | 0.4 | 0.5 | 0.2 | -4.0 | 4.0 | -0.04971 | 0.44739 | -0.13021 |
| 0.6 | 5.0 | 0.4 | 1.6 | 0.1 | 0.1 | 0.4 | 0.5 | 0.2 | -4.0 | 4.0 | -0.04971 | 0.44739 | 0.01237 |
| 0.6 | 5.0 | 0.4 | 0.8 | 0.1 | 0.1 | 0.4 | 0.5 | 0.2 | -4.0 | 4.0 | -0.04971 | 0.44739 | -0.01816 |
| 0.6 | 5.0 | 0.4 | 0.0 | 0.1 | 0.1 | 0.4 | 0.5 | 0.2 | -4.0 | 4.0 | -0.04971 | 0.44739 | -0.11171 |
| 0.6 | 5.0 | 0.4 | 0.2 | 0 | 0.1 | 0.4 | 0.5 | 0.2 | -4.0 | 4.0 | -0.49710 | 0.44739 | -0.16303 |
| 0.6 | 5.0 | 0.4 | 0.2 | 2.0 | 0.1 | 0.4 | 0.5 | 0.2 | -4.0 | 4.0 | -0.02486 | 0.44739 | -0.08982 |
| 0.6 | 5.0 | 0.4 | 0.2 | 4.0 | 0.1 | 0.4 | 0.5 | 0.2 | -4.0 | 4.0 | -0.01243 | 0.44739 | -0.08830 |
| 0.6 | 5.0 | 0.4 | 0.2 | 6.0 | 0.1 | 0.4 | 0.5 | 0.2 | -4.0 | 4.0 | -0.00829 | 0.44739 | -0.08780 |
| 0.6 | 5.0 | 0.4 | 0.2 | 0.1 | 0.1 | 0.4 | 0.5 | 0.2 | -4.0 | 4.0 | -0.04971 | 0.44739 | -0.09290 |
| 0.6 | 5.0 | 0.4 | 0.2 | 0.1 | 0.5 | 0.4 | 0.5 | 0.2 | -4.0 | 4.0 | -0.43132 | 0.38819 | -0.13625 |
| 0.6 | 5.0 | 0.4 | 0.2 | 0.1 | 1.0 | 0.4 | 0.5 | 0.2 | -4.0 | 4.0 | -0.70796 | 0.31858 | -0.19315 |
| 0.6 | 5.0 | 0.4 | 0.2 | 0.1 | 2.0 | 0.4 | 0.5 | 0.2 | -4.0 | 4.0 | -0.73876 | 0.16622 | -0.31159 |
| 0.6 | 5.0 | 0.4 | 0.2 | 0.1 | 0.1 | 0 | 0.5 | 0.2 | -4.0 | 4.0 | -0.06948 | 0.62533 | -0.15323 |
| 0.6 | 5.0 | 0.4 | 0.2 | 0.1 | 0.1 | 0.2 | 0.5 | 0.2 | -4.0 | 4.0 | -0.04084 | 0.36754 | -0.06404 |
| 0.6 | 5.0 | 0.4 | 0.2 | 0.1 | 0.1 | 0.4 | 0.5 | 0.2 | -4.0 | 4.0 | -0.03193 | 0.28740 | -0.03640 |
| 0.6 | 5.0 | 0.4 | 0.2 | 0.1 | 0.1 | 0.8 | 0.5 | 0.2 | -4.0 | 4.0 | -0.02196 | 0.19766 | -0.00916 |
| 0.6 | 5.0 | 0.4 | 0.2 | 0.1 | 0.1 | 0.4 | -2.5 | 0.2 | -4.0 | 4.0 | -0.04933 | 0.44398 | -0.09058 |
| 0.6 | 5.0 | 0.4 | 0.2 | 0.1 | 0.1 | 0.4 | -0.5 | 0.2 | -4.0 | 4.0 | -0.04971 | 0.44739 | -0.09290 |
| 0.6 | 5.0 | 0.4 | 0.2 | 0.1 | 0.1 | 0.4 | 0.5 | 0.2 | -4.0 | 4.0 | -0.05003 | 0.45024 | -0.09527 |
| 0.6 | 5.0 | 0.4 | 0.2 | 0.1 | 0.1 | 0.4 | 2.5 | 0.2 | -4.0 | 4.0 | -0.05021 | 0.45190 | -0.09051 |
| 0.6 | 5.0 | 0.4 | 0.2 | 0.1 | 0.1 | 0.4 | 0.5 | -0.4 | -4.0 | 4.0 | -0.13283 | 1.19550 | -1.06772 |
| 0.6 | 5.0 | 0.4 | 0.2 | 0.1 | 0.1 | 0.4 | 0.5 | -0.2 | -4.0 | 4.0 | -0.09503 | 0.85527 | -0.42401 |
| 0.6 | 5.0 | 0.4 | 0.2 | 0.1 | 0.1 | 0.4 | 0.5 | 0.2 | -4.0 | 4.0 | -0.04971 | 0.44739 | -0.09290 |
| 0.6 | 5.0 | 0.4 | 0.2 | 0.1 | 0.1 | 0.4 | 0.5 | 0.4 | -4.0 | 4.0 | 0.01316 | -0.11844 | 0.02084 |
| 0.6 | 5.0 | 0.4 | 0.2 | 0.1 | 0.1 | 0.4 | 0.5 | 0.2 | -1.0 | 4.0 | -0.04971 | 0.44739 | 0.28796 |
| 0.6 | 5.0 | 0.4 | 0.2 | 0.1 | 0.1 | 0.4 | 0.5 | 0.2 | -2.0 | 4.0 | -0.04971 | 0.44739 | 0.06691 |

| $\beta$ | Grt | N | $\gamma$ | Nb | Nt | $\varphi$ | $\Lambda$ | $v_0$ | G | M | $Sh$ | $Nu$ | $c_f$ |
|---|---|---|---|---|---|---|---|---|---|---|---|---|---|
| 0.6 | 5.0 | 0.4 | 0.2 | 0.1 | 0.1 | 0.4 | 0.5 | 0.2 | -3.0 | 4.0 | -0.04971 | 0.44739 | -0.00501 |
| 0.6 | 5.0 | 0.4 | 0.2 | 0.1 | 0.1 | 0.4 | 0.5 | 0.2 | -4.0 | 4.0 | -0.04971 | 0.44739 | -0.09290 |
| 0.6 | 5.0 | 0.4 | 0.2 | 0.1 | 0.1 | 0.4 | 0.5 | 0.2 | -4.0 | 4.5 | -0.04971 | 0.44739 | -0.06976 |
| 0.6 | 5.0 | 0.4 | 0.2 | 0.1 | 0.1 | 0.4 | 0.5 | 0.2 | -4.0 | 5.0 | -0.04971 | 0.44739 | -0.05410 |
| 0.6 | 5.0 | 0.4 | 0.2 | 0.1 | 0.1 | 0.4 | 0.5 | 0.2 | -4.0 | 5.5 | -0.04971 | 0.44739 | -0.04304 |

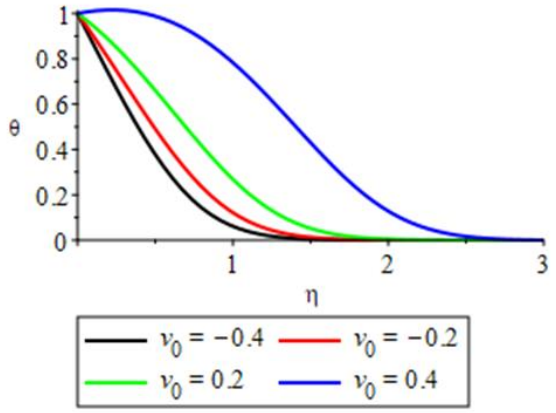


Fig.2 : Variation of Temperature distribution with $v_0$

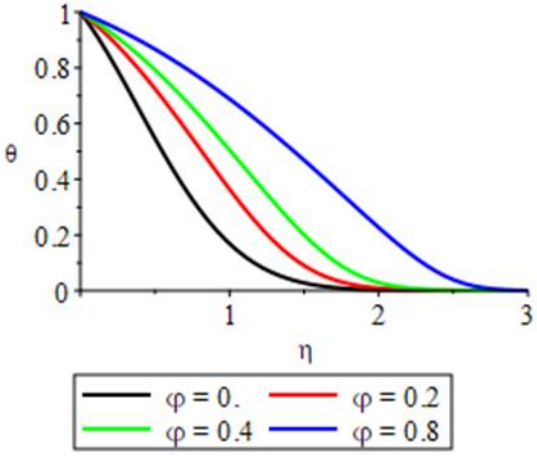


Fig.3 : Variation of Temperature distribution with $\varphi$

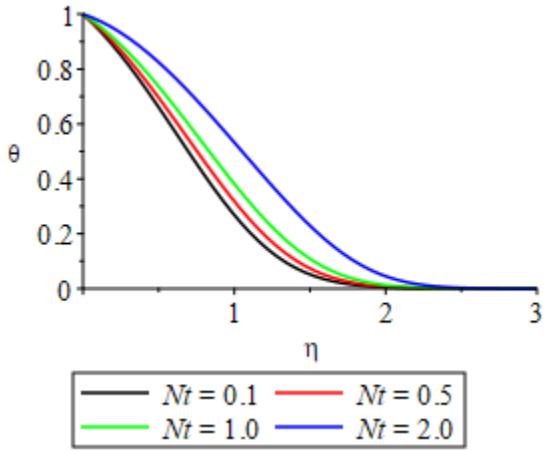


Fig.4: Variation of Temperature distribution with $Nt$

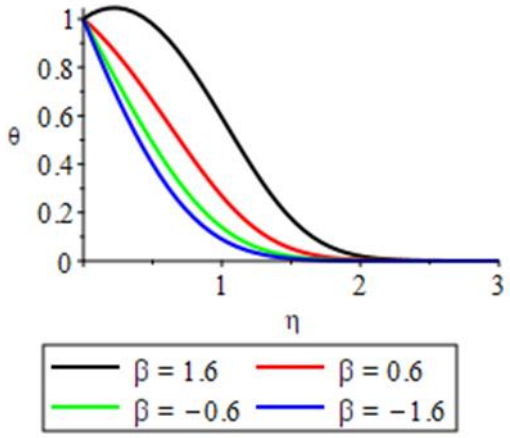


Fig.5: Variation of Temperature distribution with $\beta$

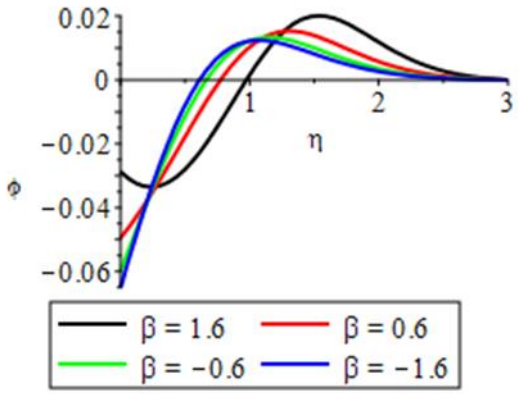


Fig.6: Variation of species concentration with $\beta$

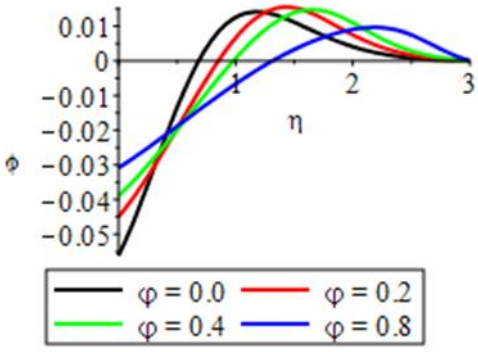


Fig.7: Variation of species concentration with $\varphi$

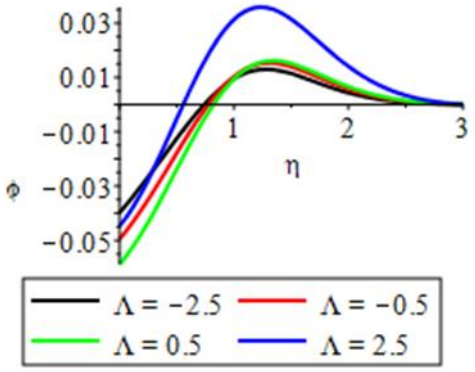


Fig.8 : Variation of species concentration with $\Lambda$

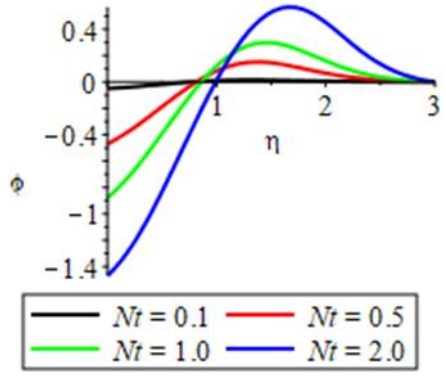


Fig.9 : Variation of species concentration with $Nt$

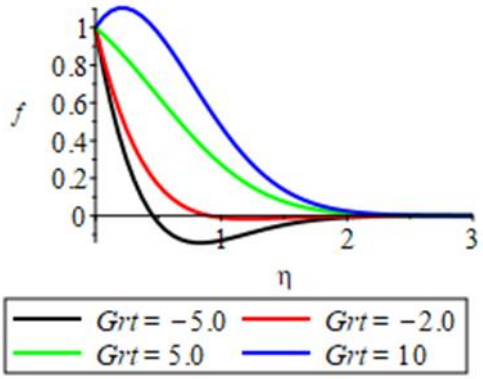


Fig.10 : Effect of $Grt$ on velocity distribution

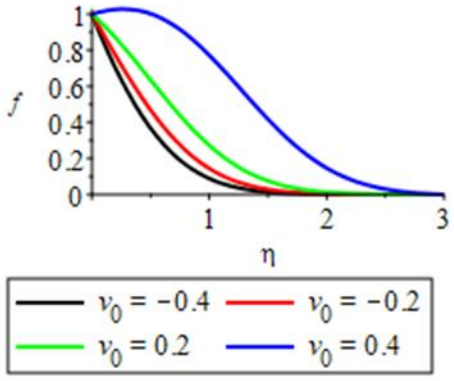


Fig.11: Effect of $v_0$ on velocity distribution

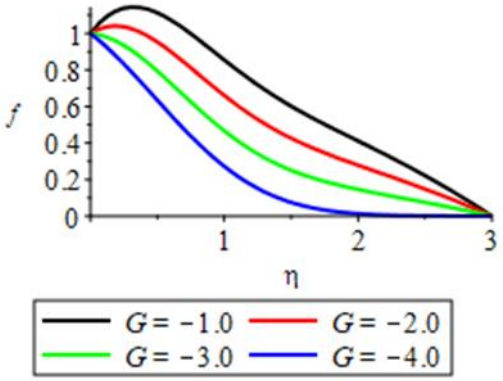


Fig.12: Effect of $G$ on velocity distribution

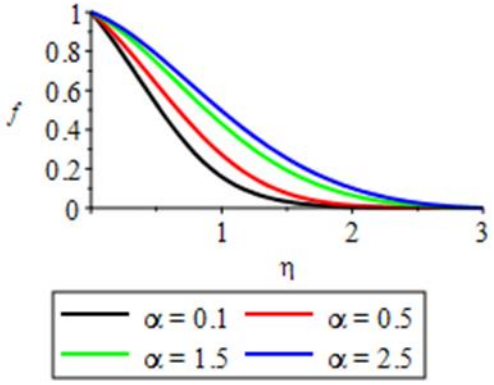


Fig.13: Effect of $\alpha$ on velocity distribution

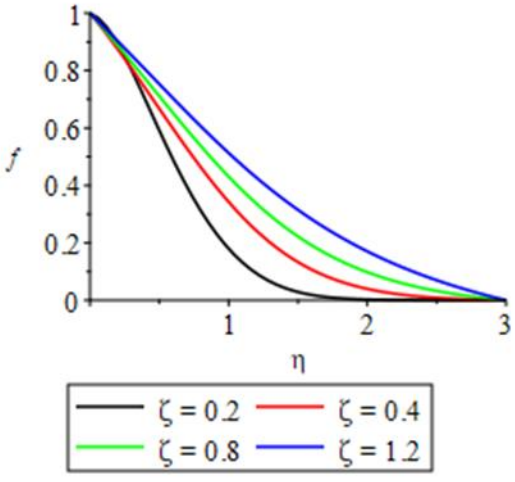


Fig.14 : Effect of $\zeta$ on velocity distribution

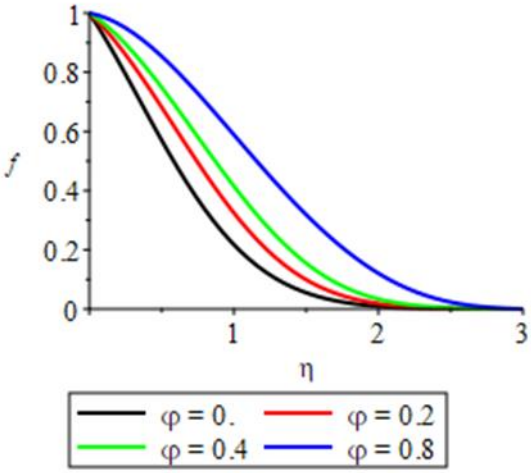


Fig.15: Effect of $\varphi$ on velocity distribution

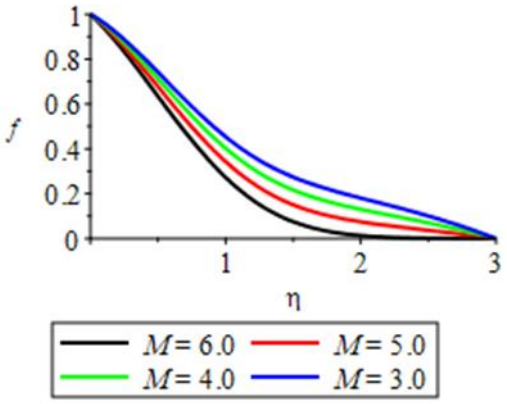


Fig.16 : Effect of $M$ on velocity distribution

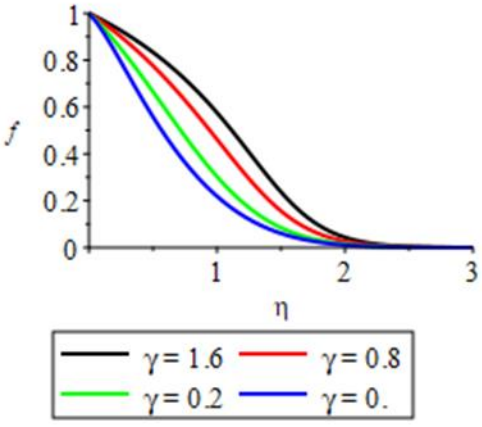


Fig.17 : Effect of $\gamma$ on velocity distribution

Appendix

| Nomenclature |
|---|

| | | | |
|---|---|---|---|
| $y$ | flow axis | $\beta_C$ | coefficient of mass expansion |
| $t$ | time | $\zeta$ | bulk viscousity |
| $u$ | velocity component along the $y-$axis | $Gr$ | Thermal Buoyancy |
| $U_\infty$ | velocity of the free stream | $M$ | Hartmann number |
| $T$ | fluid temperature | $\Lambda$ | chemical reaction parameter |
| $C$ | species concentration | $\alpha$ | bulk thermal conductivity |
| $\tau$ | Thermo-phoretic parameter | $v_0$ | suction/injection velocity |
| $E_a$ | activation energy | $Nb$ | thermophoresis parameter |
| $R_G$ | universal gas constant | $Nt$ | Brownian motion parameter |
| $\mu_T$ | temperature dependent viscousity | $N$ | buoyancy ratio |
| $k_T$ | variable thermal conductivity | $g$ | acceleration due to gravity |
| $(\rho c)_f$ | heat capacity of the nanofluid and | $\varphi$ | variable thermal conductivity |
| $T$ | fluid temperature | $\gamma$ | variable viscousity parameter |
| $C$ | nanoparticle volume fraction | G | pressure gradient |
| $U_0$ | wall shear stress $q_m =$ mass flux | $c_f$ | Skin friction |
| $q_w$ | heat transfer | $Nu$ | Nusselt Number |
| $\rho_f$ | density of base fluid | $Sh$ | Sherwood Number |
| $\nu$ | kinematic viscosity | $Pr$ | Prandtl number |
| $\sigma$ | electrical conductivity | $Sc$ | Schmidt number |
| $B_0$ | magnetic field flux density | $f$ | dimensionless flow velocity |
| $D_B$ | Brownian motion diffusion coefficient | $\theta$ | dimensionless fluid temperature |
| $D_T$ | thermophoresis diffusion coefficient | $h$ | dimensionless species concentration |
| $\beta_T$ | coefficient of thermal expansion | $w$ | condition at wall |
| $\beta$ | heat generation or absorption parameter | $\infty$ | ambient condition |
| $(\rho c)_p$ | effective heat capacity of the nanoparticle material | | |

REFERENCES


[1] Yousefi, Kianoosh and Saleh, Reza (2015): Three-dimensional suction flow control and suction jet length optimization of NACA 0012 wing. Meccanica. 50 (6): 1481–1494. https://doi:10.1007/s11012-015-0100-9

[2] Yousefi, Kianoosh; Saleh, Reza; Zahedi, Peyman (2014): Numerical study of blowing and suction slot geometry optimization on NACA 0012 airfoil. Journal of Mech Sci. and Technology. 28 (4): 1297–1310. https://doi:10.1007/s12206-014-0119-1.

[3] Filiatrault A. and Cherry S. (1990) Performance evaluation of friction dampedbraced stell frames under simulated earthquake loads."Report of Earthquake Engineering Research Laboratory, University of British Columbia, Vancouver, Canada.

[4] MD Symans, FA Charney, AS Whittaker, MC Constantinou, CA Kircher, MW Johnson, RJ McNamara. Energy dissipation systems for seismic applications: current practice and recent developments. Journal of structural engineering 134 (1), 3-21, 2008

[5] Michael D. Symans, Michael C. Constantinou (1997): Experimental Testing and Analtical Modeling of Semi-Active Fluid Dampers for Seismic Protection. Journal of Intelligent Material Systems and Structures. Vol. 8, Issue 8, pp644-657 https://doi.org/10.1177/1045389X9700800802.

[6] Tyler, R. G. (1985) Further notes on a steel energy-absorbing element for braced frameworks. Bulleting of New Zeland National Society for Earthquake Engineering. 18(3), 270-279

[7] Whittaker A. S., Bertero, V. V., Alonso, J. I. and Thompson, C. L. (1989): Earthquake simulator testing of steel plate added damping and stiffness element, Report No. UCB/EERC-89/02, University of California, Berkeley

[8] Hadar Ben-Gida, Jean Stefanini, Oksana Stalnov, Roi Gurka, Application of passive flow control techniques to attenuate the unsteady near wake of airborne turrets in subsonic flow, Aerospace Science and Technology, Volume 119, 2021, 107129, ISSN 1270-9638, https://doi.org/10.1016/j.ast.2021.107129.

[9] Omid Elhaki, Khoshnam Shojaei, A novel model-free robust saturated reinforcement learning-based controller for quadrotors guaranteeing prescribed transient and steady state performance, Aerospace Science and Technology, Volume 119, 2021, 107128, ISSN 1270-9638, https://doi.org/10.1016/j.ast.2021.107128.

[10] Tiantian Zhang, Xiaoting Yan, Wei Huang, Xueke Che, Zhenguo Wang, Enwei Lu, Design and analysis of the air-breathing aircraft with the full-body wave-ride performance, Aerospace Science and Technology, Volume 119, 2021, 107133, ISSN 1270-9638, https://doi.org/10.1016/j.ast.2021.107133.

[11] Zonghan Yu, Guoping Huang, Chen Xia, Hypersonic pressure-controllable bump based on an improved permeable-boundary method, Aerospace Science and Technology, Volume 119, 2021, 107132, ISSN 1270-9638, https://doi.org/10.1016/j.ast.2021.107132. (https://www.sciencedirect.com/science/article/pii/S1270963821006428)

[12] Eiman B. Saheby, Xing Shen, Guoping Huang, Anthony P. Hays, Flow structure of the ridge integrated submerged inlet, Aerospace Science and Technology, Volume 119, 2021, 107136, ISSN 1270-9638, https://doi.org/10.1016/j.ast.2021.107136.

[13] Farid C. Christo, Yeshayahou Levy, Mário Costa, Gabrian A.F. Balelang, Effect of jet momentum flux and heat density on NOx emission in a flameless gas turbine combustor, Aerospace Science and Technology, Volume 119, 2021, 107137, ISSN 1270-9638, https://doi.org/10.1016/j.ast.2021.107137.

[14] Tiancai Wu, Honglun Wang, Yue Yu, Yiheng Liu, Jianfa Wu, Hierarchical fault-tolerant control for over-actuated hypersonic reentry vehicles, Aerospace Science and Technology, Volume 119, 2021, 107134, ISSN 1270-9638, https://doi.org/10.1016/j.ast.2021.107134.

[15] S.T. Mohyud-Din, U. Khan, N. Ahmed, Bandar Bin-Mohsin (2017): Heat and mass transfer analysis for MHD flow of nanofluid in convergent/divergent channels with stretchable walls using Buongiorno's model, Neural Comput. Appl. 28 (12), 4079–4092.

[16] U. Khan, N. Ahmed, S.T. Mohyud-Din (2016): Stoke's first problem for carbon nanotubes suspended nanofluid flow under the effect of slip boundary condition, Journal of Nano-fluids 5 239–244.

[17] H. Schlichting, in: Boundary-Layer Theory, 6th ed., McGraw-Hill, New York, 1968.

[18] K.R. Rajagopal, T.Y. Na, On Stokes' problem for a nonNewtonian fluid, Acta Mech. 48 (1983) 233–239.

[19] M. Turkyilmazoglu, Analytical solutions of single and multiphase models for the condensation of nanofluid film flow and heat transfer, Eur. J. Mech. - B/Fluids 53 (2015) 272–277.

[20] M. Turkyilmazoglu (2012): Soret and heat source effects on the unsteady radiative MHD free convection flow from an impulsively started infinite vertical plate, Int. J. Heat. Mass Transf. 55 (25-26), 7635–7644.

[21] G.S. Seth, M.S. Ansari, R. Nandkeolyar (2011): MHD natural convection flow with radiative heat transfer past an impulsively moving plate with ramped wall temperature, Heat. Mass Transf. 47, 551–561.

[22] G.S. Seth, G.K. Mahato, S. Sarkar, M.S. Ansari (2012): Effects of Hall current on hydromagnetic natural convection flow of a heat absorbing fluid

past an impulsively moving vertical plate with ramped temperature, J. Appl. Fluid Mech. 1 (4) 462–486.

[23] G.S. Seth, R. Nandkeolyar, M.S. Ansari, Effects of thermal radiation and rotation on unsteady hydromagnetic free convection flow past an impulsively moving vertical plate with ramped temperature in a porous medium, J. Appl. Fluid Mech. 6 (1) (2013) 27–38.

[24] R. Nandkeolyar, G.S. Seth, O.D. Makinde, P. Sibanda, M.S. Ansari, Unsteady hydromagnetics natural convection flow of a dusty fluid past an impulsively moving vertical plate with ramped temperature in the presence of thermal radiation (9pages), ASME J. Appl. Mech. 80 (6) (2013) 061003, http://dx.doi.org/10.1115/1.4023959.

[25] G.S. Seth, S. Sarkar, S.M. Hussain, Effects of Hall current, radiation and rotation on natural convection heat and mass transfer flow past a moving vertical plate, Ain Shams Eng. J. 5 (2014) 489–503.

[26] G.S. Seth, S. Sarkar, S.M. Hussain, G.K. Mahato, Effects of Hall current and rotation on hydromagnetic natural convection flow with heat and mass transfer of a heat absorbing fluid past an impulsively moving vertical plate with ramped temperature, J. Appl. Fluid Mech. 8 (1) (2015) 159–171.

[27] G.S. Seth, S. Sarkar, MHD natural convection heat and mass transfer flow past a time dependent moving vertical plate with ramped temperature in a rotating medium with Hall effects, radiation and chemical reaction, J. Mech. 31 (2015) 91–104.

[28] G.S. Seth, S. Sarkar, R. Sharma (2016): Effects of Hall current on unsteady hydromagnetic free convection flow past an impulsively moving vertical plate with Newtonian heating, Int. J. Appl. Mech. Eng. 21 (1) 187–203.

[29] G.S. Seth, S. Sarkar (2015): Hydromagnetic natural convection flow with induced magnetic field and nth order chemical reaction of a heat absorbing fluid past an impulsively moving vertical plate with ramped temperature, Bulg. Chem. Commun. 47 (1) 66–79.

[30] V.M. Soundalgekar, Stokes problem for elastico-viscous fluid, Rheol. Acta 13 (1981) 177–179.

[31] P. Puri, Impulsive motion of a flat plate in a Rivlin-Ericksen fluid, Rheol. Acta 23 (1984) 451–453.

[32] P. Puri, M. Jordan, Stokes's first problem for a dipolar fluid with non-classical heat conduction, J. Eng. Math. 36 (1999) 219–240.

[33] N. Uddin, W.A. Khan, M. Rahi (2012): Heat and mass transfer from a suddenly moved plate in nano fluids, Proc. Inst. Mech. Eng., Part N: J. Nanoeng. Nanosyst.1–9, http://dx.doi.org/10.1177/1740349912456786.

[34] H. Rosali, A. Ishak, I. Pop, Stokes' first problem in nanofluids, Curr. Nanosci. 10 (2014) 409–413.

[35] D.A. Nield, A.V. Kuznetsov (2014): The onset of convection in a horizontal nanofluid layer of finite depth: a revised model, Int. J. Heat. Mass Transf. 77 915–918.

[36] D.A. Nield, A.V. Kuznetsov, Natural convective boundarylayer flow of a nanofluid past a vertical plate: a revised model, Int. J. Therm. Sci. 77 (2014) 126–129.

[37] D.A. Nield, A.V. Kuznetsov, Thermal instability in a porous medium layer saturated by a nanofluid: a revised model, Int. J. Heat. Mass Transf. 68 (2014) 211–214.

[38] Syed Tauseef ,Mohyud-Din, Umar Khan, Naveed Ahmed, Muhammad Mehdi Rashidi: A study of heat and mass transfer on magnetohydrodynamic (MHD) flow of nanoparticles Propulsion and Power Research 2018;7(1):72–77)

[39] A. M. Okedoye and P. O. Ogunniyi (2019): MHD Boundary Layer Flow Past a Moving Plate with Mass Transfer and Binary Chemical Reaction. Journal of the Nigerian Mathematical Society, Vol. 38, Issue 1, pp. 89-121.

[40] A. M. Okedoye and S. O. Salawu (2019): Unsteady oscillatory MHD boundary layer flow past a moving plate with mass transfer and binary chemical reaction. SN Applied Sciences (2019) 1:1586 https://doi.org/10.1007/s42452-019-1463-7.

[41] Akindele M. Okedoye and Sulyman O. Salawu (2019): Effect of Nonlinear Radiative Heat and Mass Transfer on MHD Flow over a Stretching Surface with Variable Conductivity and

Viscosity. Journal of the Serbian Society for Computational Mechanics / Vol. 13 / No. 2, 2019 / pp 86-103 https://doi:10.24874/jsscm.2019.13.02.07.

[42] A.M. Okedoye and S.O. Salawu (2020): transient heat and mass transfer of hydromagnetic effects on the flow past a porous medium with movable vertical permeablesheet. Int. J. of Applied Mechanics and Engineering, 2020, vol.25, No.4, pp.175-190. https://doi:10.2478/ijame-2020-0057.

[43] Hafiz Abdul Wahab, Hussan Zeb, Saira Bhatti, Muhammad Gulistan, Seifedine Kadry and Yunyoung Nam: Numerical Study for the Effects of Temperature Dependent Viscosity Flow of Non-Newtonian Fluid with Double Stratification. *Appl. Sci.* 2020, *10*, 708; http://dx.doi.org/10.3390/app10020708